Letter

Highly confined, low-loss plasmonics based on two-dimensional solid-state defect lattices

Ali Ghorashi,[1] Nicholas Rivera,[1,2] Bowen Shi,[1,3] Ravishankar Sundararaman,[4] Efthimios Kaxiras,[5,2] John Joannopoulos,[1,6] and Marin Soljačić[1]

[1]*Department of Physics, Massachusetts Institute of Technology, Cambridge, Massachusetts 02139, USA*
[2]*Department of Physics, Harvard University, Cambridge, Massachusetts 02134, USA*
[3]*State Key Laboratory for Mesoscopic Physics and Department of Physics, Peking University, Beijing 100871, People's Republic of China*
[4]*Materials Science and Engineering, Rensselaer Polytechnic Institute, Troy, New York 12180, USA*
[5]*School of Engineering and Applied Sciences, Harvard University, Cambridge, Massachusetts 02134, USA*
[6]*Institute for Soldier Nanotechnologies, Massachusetts Institute of Technology, Cambridge, Massachusetts 02139, USA*

(Received 2 May 2023; accepted 18 December 2023; published 8 January 2024)

Plasmons, collective excitations of electrons in solids, are associated with strongly confined electromagnetic fields, with wavelengths far below the wavelength of photons in free space. Such strong confinement nominally holds the potential to enable optoelectronic technologies that bridge the size difference between photonic and electronic devices. However, despite decades of research in plasmonics, many applications remain limited by plasmonic losses, thus motivating a search for new engineered plasmonic materials with lower losses. Among the promising candidates for low-loss plasmonic materials are solid-state lattices with flat and energetically isolated metallic bands—with commensurately small phase spaces for phonon-assisted optical losses, a major contributor to short plasmonic lifetimes. Such electronic band structures may be created by judiciously introducing an ordered lattice of defects in an insulating host material. Here, we explore this approach, presenting several low-loss, highly confined, and tunable plasmonic materials based on arrays of carbon substitutions in hexagonal boron nitride monolayers. From our first-principles calculations based on density functional theory, we find plasmonic structures with midinfrared plasmons featuring very high confinements ($\lambda_{\text{vacuum}}/\lambda_{\text{plasmon}}$ exceeding 1400). In addition, we find that one of our materials exhibits a confinement of 700 while avoiding second-order—phonon-assisted—losses entirely (infinite quality factor at this order of perturbation theory). We provide a systematic explanation of how crystal structure, electronic bandwidth, local-field, and many-body effects inform the plasmonic dispersions and losses of these materials. The results are thus of relevance to low-loss plasmon engineering in other flat band systems.

DOI: 10.1103/PhysRevMaterials.8.L011001

The optoelectronic properties of two-dimensional (2D) materials are of major interest due to the qualitatively different physics of electron-photon interactions in reduced dimensions. Accordingly, the search for stable 2D materials with specific optoelectronic properties has been a topic of intense research in recent years [1–3]. In particular, the expansion of the repertoire of stable 2D materials has made strides in three directions:

(i) The tuning of geometric properties of van der Waals (vdW) bilayers and trilayers, most notably by creating moiré patterns [4];

(ii) the advent or prediction of 2D analogues of naturally occurring three-dimensional metals [5,6]; and

(iii) the introduction of defects in common 2D materials [1] to induce desired optoelectronic properties.

A major impetus has been to enable collective excitations, such as plasmons [7], phonon polaritons [8,9], and exciton polaritons [10], with tailored dispersions, high confinements, and/or low losses [11], which would enable a wide range of new light-matter interaction effects [12,13]. In the case of plasmons specifically, whose electromagnetic fields can be confined far below the free-space wavelength of photons, many of the promising applications envisioned for the field decades ago are still hindered to this day by loss. Strongly confined and low-loss plasmonic excitations could lead to major advances for most envisioned applications of plasmonics in fields spanning photovoltaics [14], spectroscopy [15], biosensing [16], and ultrahigh resolution lasers [17].

Our study is motivated by the goal of significantly reducing the ubiquitous losses intrinsic to plasmonic materials [18,19]. In particular, we focus on 2D materials whose metallic character is *induced* by the presence of defects [an example of case (iii) above]. To avoid loss channels such as interband transitions, we restrict our search to a host material with a large band gap, namely, hexagonal boron nitride (hBN) (6 eV band gap; see [20]), and defects that produce moderately flat bands near the middle of the band gap.[1] For the defects, we choose carbon atoms since their atomic size, similar to that of B and N, minimizes defect-induced lattice strain. The substitutional defect structures that we consider are denoted as $C_X^{n\times n}$, indicating an $n \times n$ supercell of the primitive unit cell of hBN, in which one atom labeled X is replaced by a C atom [an example of which is shown in Fig. 1(b)]. We

[1]A truly flat band does not support plasmonic excitations and a highly dispersive band increases intraband losses.

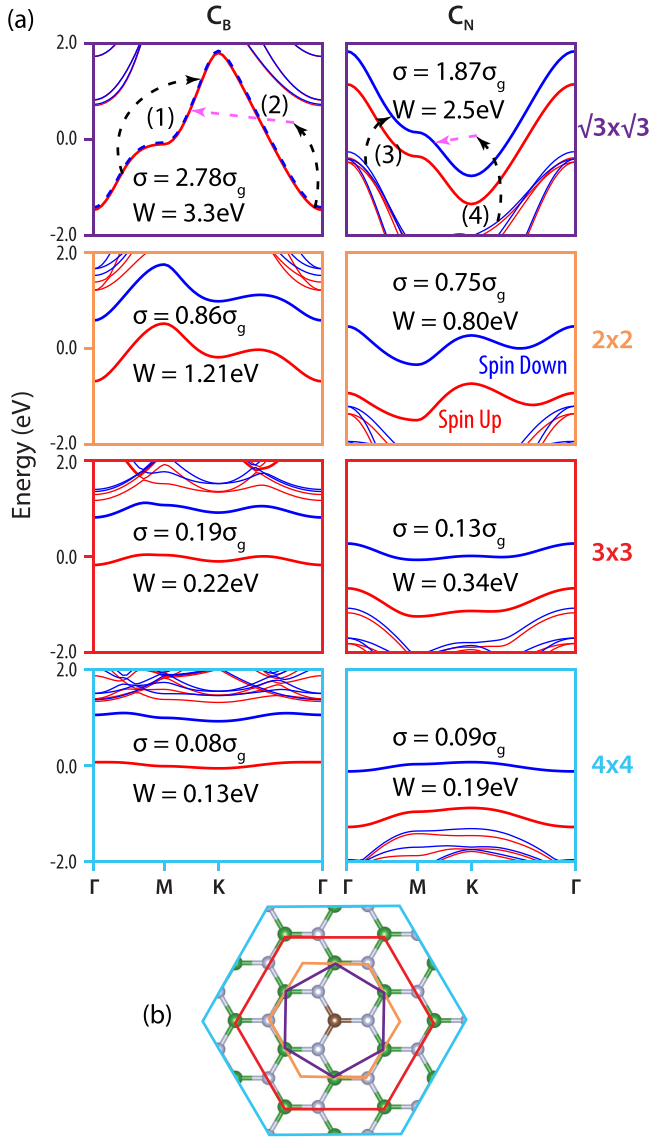

FIG. 1. Electronic band structures. (a) Electronic bands for $C_B^{n\times n}$ (left column) and $C_N^{n\times n}$ (right column) structures. Energy is measured from the Fermi level. For the six lattices that are insulating and ferromagnetic, we shift the Fermi energy to half filling of the defect band closest to the hBN midgap. We report the bandwidth W and conductivity σ for each structure (σ_g is graphene's conductivity at 0.5 eV doping). The labels (1) and (3) denote intraband and interband Landau damping processes, respectively. The labels (2) and (4) denote interband and interband phonon-assisted damping processes, respectively. Black dashed lines denote plasmons and pink dashed lines denote phonons. (b) The Wigner-Seitz cells for the four structures that we considered, within the largest 4×4 structure. The brown circle denotes the C defect at the center of the cell. White circles denote N atoms for the B substitutional lattices and B atoms for the N substitutional lattices. Green circles denote B atoms for the B substitutional lattices and N atoms for the N substitutional lattices. The color scheme is the same as in (a) with purple, orange, red, and light blue corresponding to $\sqrt{3} \times \sqrt{3}$, 2×2, 3×3, and 4×4, respectively.

study supercells with $n = \sqrt{3}, 2, 3, 4$ and $X =$ B or N, that is, a total of eight defect-containing structures. Typically, larger supercells can host flatter bands, which are more conducive to low-loss plasmonics.

The eight structures and corresponding electronic band structures are shown in Fig. 1. Our density functional theory (DFT) calculations indicate that the relaxed structures with N substitutional atoms are perfectly planar, whereas those with B are slightly buckled; see the Supplemental Material (SM) [21]. While this is a minor structural difference, we show later that it has a significant impact on the magnitude of the electron-phonon interaction. All of the structures, other than the two $C_X^{\sqrt{3}\times\sqrt{3}}$ ones, are fully spin polarized, meaning that they must be doped in order to support plasmons. As previously predicted [22,23], we find that the structures with larger supercells are ferromagnetic, with spin gaps of the order of 1 eV.[2] The structures we report have bandwidths ranging from 3.3 eV ($C_B^{\sqrt{3}\times\sqrt{3}}$) to 0.13 eV ($C_B^{4\times4}$).[3] This decrease in the bandwidth as lattice size is increased is accompanied by a commensurate decrease in the Fermi velocity and the onset of ferromagnetism (lifting of spin degeneracy), both of which contribute to a lowering of the Drude conductivity as seen in Fig. 1(a). This then leads to lower frequency plasmons for the larger defect supercells.

Limiting plasmonic losses has been an active area of research for several decades [24]. In all proposed candidates for low-loss plasmonics, losses are mitigated by suppressing the phase space for direct and indirect (phonon-assisted) transitions into the electron-hole continuum. In the case of surface plasmons, for instance, one early proposal for avoiding losses was by engineering semiconducting superlattices that energetically separate the plasmonic band from the electron-hole continuum [24]. In the case of our structures that include substitutional defects, a similar energetic separation should exist, as the structures with larger periodicity host flat bands that are well separated from the hBN valence and conduction bands. Accordingly, we calculate the transverse magnetic (TM) polarized plasmonic dispersions and associated losses in the proposed structures. For the $C_B^{\sqrt{3}\times\sqrt{3}}$ and $C_N^{\sqrt{3}\times\sqrt{3}}$ structures, which are metallic at charge neutrality, we calculate the plasmonic properties without imposing any changes in band occupation. For the structures with larger supercells, we move the Fermi level to half filling of the defect band closest to the hBN midgap and calculate plasmonic properties within the rigid band approximation [25], which neglects changes to the band structure due to doping (we analyze the validity of this approximation below).

We calculate the plasmon dispersion through the poles of the inverse dielectric function, $\varepsilon^{-1}(\mathbf{q}, \omega)$, which at finite temperature is given by [26]

$$\frac{1}{\varepsilon(\mathbf{q}, i\omega_n)} = 1 - \frac{V_\mathbf{q}}{N_\mathbf{k}\Omega} \int_0^\beta e^{i\omega_n \tau} \langle \mathcal{T}\rho(\mathbf{q}, \tau)\rho(-\mathbf{q}, 0)\rangle \, d\tau, \tag{1}$$

[2]To verify their ferromagnetic order, we calculate the ground state of a 2×2 supercell of $C_B^{2\times2}$ and find that the ferromagnetic state is preferred, with magnetization $4\mu_B$.

[3]For comparison, we calculated the bandwidth with the LDA [31] and PBESol [38] functionals for $C_B^{3\times3}$ as well and found it varied by, at most, 10 meV.

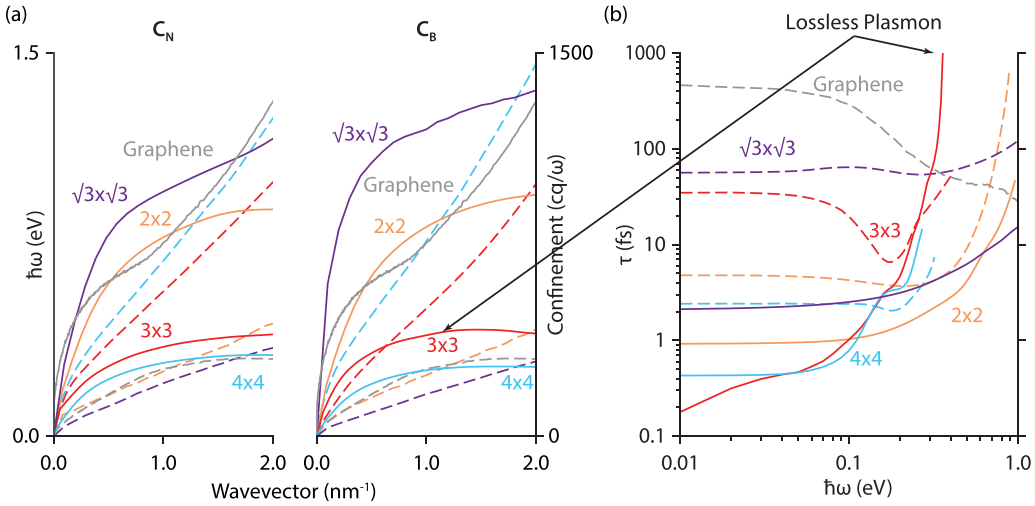

FIG. 2. Plasmonic dispersions, confinements, and losses. (a) Plasmonic dispersions (solid lines) and confinements (dashed lines) compared to graphene. Wave vectors were chosen to lie on the $\Gamma - M$ direction. (b) Decay times for $C_B^{n\times n}$ ($C_N^{n\times n}$) in solid (dashed) lines and graphene at 0.5 eV doping (dashed gray line).

where Ω is the unit cell area, $N_{\mathbf{k}}$ is the number of sampled Brillouin zone points, $\mathcal{T}$ is the imaginary-time ordering operator, $\mathbf{q}$ is the wave vector, and $V_{\mathbf{q}} = \frac{e^2}{2\epsilon_0 \mathbf{q}}$ is the Coulomb interaction in 2D (with ϵ_0 the vacuum permittivity), β is the inverse temperature, and $\rho(\mathbf{q}, \tau)$ is the density operator in the Heisenberg representation. Equation (1) yields the inverse dielectric function at a bosonic Matsubara frequency, ω_n. The retarded inverse dielectric function is then calculated by analytically continuing $i\omega_n \to \omega + i\delta$. We note that though Eq. (1) includes the full directional dependence of the system response, in the local $\mathbf{q} \to 0$ limit, the C_3 symmetry of our lattices enforces the conductivity and dielectric function to be isotropic (see the SM [21]).

Electron-electron interactions are included through the random phase approximation (RPA) [26], which gives the standard result (neglecting local-field effects) [27],[4]

$$\varepsilon(\mathbf{q}, \omega) = 1 - \frac{e^2}{2\varepsilon_0 \mathbf{q} N_{\mathbf{k}} \Omega} \mathcal{F}(\mathbf{q}, \omega), \tag{2}$$

$$\mathcal{F}(\mathbf{q}, \omega) = \sum_{k,n,m} \frac{f\left(\epsilon^n_{\mathbf{k}+\mathbf{q}}\right) - f\left(\epsilon^m_{\mathbf{k}}\right)}{\epsilon^n_{\mathbf{k}+\mathbf{q}} - \epsilon^m_{\mathbf{k}} - \hbar\omega - i\delta} |\langle \mathbf{k}+\mathbf{q}, n | \mathbf{k}, m\rangle|^2, \tag{3}$$

where $\langle \mathbf{k}+\mathbf{q}, n|, |\mathbf{k}, m\rangle$ denote the cell periodic components of the Kohn-Sham eigenstates with corresponding energy eigenvalues $\epsilon^n_{\mathbf{k}+\mathbf{q}}, \epsilon^m_{\mathbf{k}}$ and $f(\epsilon)$ is the Fermi occupation. We note that in Eq. (3), the spin indices are subsumed into the band indices, m, n. One additional wrinkle in our calculations is that since we use a Wannier tight-binding basis to compute overlaps, we have to take into account the locations of the Wannier orbitals in computing $|\langle \mathbf{k}+\mathbf{q}, n | \mathbf{k}, m\rangle|^2$,

$$\langle \mathbf{k}+\mathbf{q}, n | \mathbf{k}, m\rangle = \sum_u e^{i\mathbf{q}\cdot\tau_u} U^{\mathbf{k}+\mathbf{q}}_{nu} \left(U^{\mathbf{k}}_{mu}\right)^*, \tag{4}$$

where the $U^{\mathbf{k}}_{ij}$ are the Wannier unitary rotation matrices and τ_i the locations of the Wannier orbitals within the unit cell (see SM [21]). We note that such local-field effects become important when the locations of the Wannier orbitals in the unit cell become comparable to the plasmonic wavelength. We report plasmonic dispersions and confinements in Fig. 2(a) as compared to the most well-established 2D plasmonic platform, i.e., graphene, at 0.5 eV doping from the Dirac point. The plasmons in the proposed structures cover a frequency range from 0 to ~1.4 eV, with plasmons below 1 eV immune to interband and intraband Landau damping—first-order—losses (see SM [21]). These plasmons have confinements in the plotted wave-vector range of up to ~5 times that of graphene (for the $C_B^{4\times4}$ structure). We note that the generically small plasmonic group velocities observed for most of the proposed structures are a consequence of interband screening, a nearly universal phenomenon in 2D [28]. This is not the case for the $C_B^{\sqrt{3}\times\sqrt{3}}$ and $C_N^{\sqrt{3}\times\sqrt{3}}$ structures, as in those cases the plasmon approaches the interband continuum at large wave vectors.

We calculate the plasmonic phonon-induced decay rate at second order in perturbation theory (see SM [21]):

$$\tau^{-1}(\omega) = \frac{2\pi}{N_{\mathbf{k}} N_{\mathbf{k}'} \hbar^2 \omega g(\epsilon_F)} \sum_{\mathbf{k},\mathbf{k}' j\pm} \left|g^j_{\mathbf{k},\mathbf{k}'}\right|^2 \left(N^{j,\mp}_{\mathbf{k}-\mathbf{k}'} f_{\mathbf{k}} - N^{j,\pm}_{\mathbf{k}-\mathbf{k}'} f_{\mathbf{k}'} \pm f_{\mathbf{k}} f_{\mathbf{k}'}\right) \delta\left(\epsilon_{\mathbf{k}} + \hbar\omega \pm \hbar\omega^j_{\mathbf{k}-\mathbf{k}'} - \epsilon_{\mathbf{k}'}\right) \times \left(1 - \frac{v_{\mathbf{k}} \cdot v_{\mathbf{k}'}}{|v_{\mathbf{k}}||v_{\mathbf{k}'}|}\right), \tag{5}$$

where $v_{\mathbf{k}}$, $v_{\mathbf{k}'}$ are the electronic velocities at wave vectors $\mathbf{k}$ and $\mathbf{k}'$, respectively, $\omega^j_{\mathbf{q}}$ are the phonon frequencies of branch j at wave vector q, with corresponding $N^j_{\mathbf{q}}$ Bose occupation factors. In Eq. (5), we have defined the quantities

$$N^{j,\pm}_{\mathbf{q}} \equiv \tfrac{1}{2} + N^j_{\mathbf{q}} \pm \tfrac{1}{2},$$

where the plus (minus) sign corresponds to phonon emission (absorption). We sum over phonon bands, indexed by j,

[4]In the present work, we disregarded local-field effects [39,40], which are likely substantial only when $|q| = |q + G|$, where G is a reciprocal lattice vector.

but we include only the defect-related electronic band in the evaluation of the decay rate from Eq. (5), which is an exact expression in the frequency regime of interest (0–1 eV).

In Fig. 2(b), we present phonon-induced plasmonic decay times, $\tau(\omega)$. The $C_N^{\sqrt{3}\times\sqrt{3}}$ and $C_N^{2\times2}$ lattices yield better plasmonic lifetimes than graphene at high frequencies, with $C_N^{\sqrt{3}\times\sqrt{3}}$ plasmons having lifetimes about four times those of graphene plasmons at $\sim$1 eV. It should be noted that at such frequencies, graphene is also highly Landau damped (of the order of femtoseconds), so our order of a few improvement in phonon-induced decay times is in fact a major underestimate (but a fairer comparison). The fact that the decay times are lower for the B substitutional structures is due to enhancement of the electron-phonon interaction through the aforementioned buckling of the C_B structures. We verified this by explicitly comparing the decay times for buckled and unbuckled (nonrelaxed) C_B structures (see SM [21]). However, though the B substitutional lattices have lower quality factors in general, $C_B^{3\times3}$ actually evades loss at high frequencies—at frequencies exceeding 0.37 eV, there are no energy-conserving loss processes for this material. In particular, at a wave vector of 1.4 nm^{-1}, we find that $C_B^{3\times3}$ has plasmon of frequency 0.417 eV. To determine how reasonable our lossless plasmon is, we accounted for the most likely source of error—convergence with respect to the number of Wannier bands—by calculating the interband dielectric function of pure hBN with 20 bands (corresponding to 180 bands in a 3×3 supercell). This then gave an indication of how much the plasmon dispersion would decrease. We found that with this estimate, the plasmon would be lowered from 0.417 to 0.4 eV, but not below the second-order loss threshold of 0.37 eV. In addition, we expect that the underestimation of the hBN band gap from DFT would work in our favor in an experimental setting, as the true dielectric screening from interband transitions would be significantly lower.

As shown in the Supplemental Material [21], we calculate the expected decay time in the region where one-phonon processes are disallowed—this calculation being a result of 13 Feynman diagrams that contribute at third order in perturbation theory. Our calculations indicate that the two-phonon plasmonic decay process strongly depends on the electronic self-energies. Due to the strong electron-phonon interaction, we found the imaginary part of the electronic self-energy to be around 1–10 eV at room temperature, corresponding to a plasmonic lifetime of about 10^8 fs.

Though a subset of our materials have plasmons with quality factors that exceed those of graphene plasmons in small frequency ranges, graphene still enables overall higher quality plasmons for most frequencies. This is attributed to the fact that in the carrier decay rate, the density of states effectively shows up twice in the numerator and once in the denominator (see SM [21]). Thus, as a flat band hosts a tightly confined (in frequency) region with a high density of states, our observation of a small decay time at low frequencies is to be expected. In addition, the fact that flatter bands in general host lower frequency plasmons results in plasmons being pushed into the regime of high loss. In view of this, the $C_B^{3\times3}$ lattice straddles a lucky middle ground: its band structure is sufficiently flat to limit the phase space of phonon-induced loss, but not too flat so as not to be able to enable plasmonic excitations that enter this phase space.

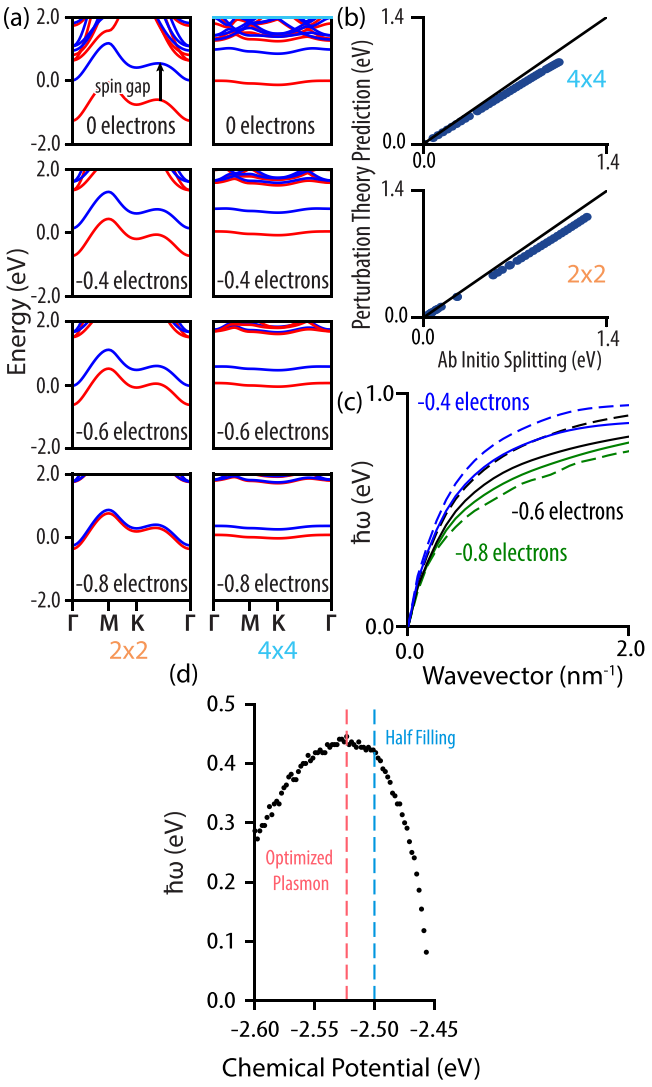

FIG. 3. Doping effect on band structures and plasmonic dispersions. (a) Band structures near the Fermi level as a function of doping for $C_B^{2\times2}$ (left column) and $C_B^{4\times4}$ (right column). (b) Accuracy of our spin-splitting model given by Eq. (6). Each blue dot represents a DFT calculation for which we plot our predicted spin splitting against the DFT result. The proximity of each point to the $y=x$ line (shown in black) indicates the validity of the perturbation theory model. (c) Plasmonic dispersion for $C_B^{2\times2}$ at various values of doping calculated in the rigid band approximation (dashed lines) and from the explicit charged DFT calculations (solid lines). (d) Calculation of plasmon dispersion for $C_B^{3\times3}$ at various degrees of rigid doping.

We turn next to the promised validity check of the rigid band approximation, which we have heretofore implicitly used. Interestingly, we find that electron and hole doping in the structures we consider has the effect of tuning the spin gap at the Fermi level [see Fig. 3(a)], which is at odds with the bands being rigidly doped. We attribute this result to changes in the exchange potential with respect to doping. In particular, the exchange potential in DFT is a functional of the

spin-resolved electron densities. From perturbation theory in the local density approximation (LDA), the doping results in a spin gap are given by (see SM [21])

$$\Delta[\rho_\uparrow(r),\rho_\downarrow(r)] = \left(\frac{6}{\pi}\right)^{1/3} \int \left[\rho_\uparrow^{1/3}(r) - \rho_\downarrow^{1/3}(r)\right] \times \frac{[|\psi_\uparrow(r)|^2 + |\psi_\downarrow(r)|^2]}{2} d^3r, \quad (6)$$

where $\rho_\uparrow$, $\rho_\downarrow$ and $\psi_\uparrow$, $\psi_\downarrow$ are the spin-up (-down) densities and wave functions, respectively. We evaluate the reliability of this model by performing DFT calculations on the doped structures as shown in Fig. 3(b). For each material, we use three functionals: Perdew-Burke-Ernzerhof generalized gradient approximation (PBE-GGA) [29], Slater LDA without correlation [30], and LDA with correlation [31]. For each value of doping, we calculate the spin splitting from DFT at the Γ point (center of the Brillouin zone in reciprocal space). We also use the self-consistent density and the Kohn-Sham wave functions for the defect bands to calculate the predicted spin-splitting value given by Eq. (6). In Fig. 3(b), we plot our prediction against the exact DFT values. The plots in Fig. 3(b) are obtained by using the PBE-GGA exchange-correlation functional for the structures $C_B^{2\times2}$ and $C_B^{4\times4}$. As is evident, the fit of our model to the numerical DFT results is very accurate. We present analogous plots for the other two functionals and for all other lattices in the SM [21].

In Fig. 3(c), we show plasmonic dispersions as a function of doping. We find that the explicitly doped plasmons differ quantitatively from those obtained through the rigid band approximation by about 10% at most, with the best agreement being for the systems doped at −0.8 electrons per unit cell. Interestingly, we find that discarding Wannier local-field effects results in a much worse agreement between the rigidly doped and explicitly doped plasmonic dispersions, which is another testament to their importance. We investigated the origin of the quantitative discrepancies shown in Fig. 3(c) and found the major contributing factors to be differences in wave-function overlaps between bands separated by large frequencies, most likely due either to the fact that the Wannier convergence window does not cover conduction bands far from the Fermi level or to the fact that the neutralizing background charge in the explicitly doped computations may change the nature of the Kohn-Sham wave functions. To better understand how doping affects the plasmonic bands, other physically motivated scenarios for doping, such as through lithium intercalation [32], need to be investigated, as a uniform neutralizing charge does not reflect an experimentally realizable doping mechanism.

The prospect of doping raises another question: Can one dope the $C_B^{3\times3}$ system such that its "lossless" plasmon is pushed even further into the lossless regime? To answer this question, we rigidly doped the $C_B^{3\times3}$ system and calculated the plasmon dispersion at the wave vector that provided the highest plasmon frequency at half filling, as shown in Fig. 3(d). We found the maximum plasmon frequency can reach up to 0.45 eV through doping (well above the phonon-induced loss phase space).

In conclusion, we have introduced a set of candidate 2D materials with different plasmonic properties, consisting of doped hBN through C substitution at either B or N sites. In particular, we predict these structures to host plasmons with confinements up to five times the maximum achievable in graphene, with decay times that can also surpass that of graphene, for frequency ranges exceeding ∼0.4 eV. In addition, we predict that one of our materials could entirely evade the lowest-order phonon loss mechanism.

We expect that imperfections in the periodicity of these materials will not have qualitative consequences as long as the density of defects is similar to the superlattices that we investigated. However, this issue and the effect of impurities [33] is a topic for future investigation.

As most of the proposed structures have low Fermi velocities, it is possible that their electron-electron interactions necessitate an approach beyond RPA. Investigation of the validity of the random phase approximation in treating these flat band systems and their collective excitations warrants further investigation. Similar work, which explored beyond RPA diagrams in the case of graphene [34], has already been done, but not applied to defect structures of the type considered here. The effect of the electron-plasmon interaction on the carrier lifetimes should also be considered for a better assessment of the Drude decay time [35]. In addition, even in the absence of doping, exciton polaritons may exist in the proposed structures [36] and this needs to be further investigated.

We note, in closing, that there has recently been a flurry of work in creating databases of 2D materials [3,37]. While a "blind" enumeration of the plasmonic properties of all tabulated materials would be an overly demanding task, the results presented here suggest a simpler approach. Namely, we expect that filtering the available databases for materials with isolated flat bands at the Fermi level and high structural and thermal stability would be a first step in identifying the most promising candidates for low plasmonic losses.

This Letter is based upon work supported by the Air Force Office of Scientific Research under Award No. FA9550-21-1-0299, as well as in part by the U. S. Army Research Office through the Institute for Soldier Nanotechnologies at MIT, under Collaborative Agreement No. W911NF-18-2-0048. A.G. thanks the National Science Foundation Graduate Research Fellowship for financial support during the preparation of this Letter. N.R. acknowledges the support of a Junior Fellowship from the Harvard Society of Fellows, as well as earlier support from a Computational Science Graduate Fellowship of the Department of Energy (Grant No. DE-FG02-97ER25308), and a Dean's Fellowship from the MIT School of Science. E.K. is supported in part by an Army Research Office grant under Cooperative Agreement No. W911NF-21-2-0147. The authors would also like to thank Ali Fahimniya, Cyprian Lewandowski, Thomas Christensen, Marinko Jablan, and Jennifer Coulter for useful discussions.

[1] P. Huang, M. Grzeszczyk, K. Vaklinova, K. Watanabe, T. Taniguchi, K. S. Novoselov, and M. Koperski, Phys. Rev. B **106**, 014107 (2022).
[2] I. Lončarić, Z. Rukelj, V. M. Silkin, and V. Despoja, npj 2D Mater. Applicat. **2**, 1 (2018).
[3] M. N. Gjerding, A. Taghizadeh, A. Rasmussen, S. Ali, F. Bertoldo, T. Deilmann, N. R. Knøsgaard, M. Kruse, A. H. Larsen, S. Manti *et al.*, 2D Mater. **8**, 044002 (2021).
[4] C. Lewandowski and L. Levitov, Proc. Natl. Acad. Sci. **116**, 20869 (2019).
[5] R. Sundararaman, T. Christensen, Y. Ping, N. Rivera, J. D. Joannopoulos, M. Soljačić, and P. Narang, Phys. Rev. Mater. **4**, 074011 (2020).
[6] K. S. Novoselov, D. Jiang, F. Schedin, T. Booth, V. Khotkevich, S. Morozov, and A. K. Geim, Proc. Natl. Acad. Sci. **102**, 10451 (2005).
[7] S. V. Boriskina, T. A. Cooper, L. Zeng, G. Ni, J. K. Tong, Y. Tsurimaki, Y. Huang, L. Meroueh, G. Mahan, and G. Chen, Adv. Optics Photon. **9**, 775 (2017).
[8] S. Dai, W. Fang, N. Rivera, Y. Stehle, B.-Y. Jiang, J. Shen, R. Y. Tay, C. J. Ciccarino, Q. Ma, D. Rodan-Legrain *et al.*, Adv. Mater. **31**, 1806603 (2019).
[9] N. Rivera, T. Christensen, and P. Narang, Nano Lett. **19**, 2653 (2019).
[10] D. Novko, K. Lyon, D. J. Mowbray, and V. Despoja, Phys. Rev. B **104**, 115421 (2021).
[11] J. B. Khurgin, Faraday Discuss. **178**, 109 (2015).
[12] N. Rivera, I. Kaminer, B. Zhen, J. D. Joannopoulos, and M. Soljačić, Science **353**, 263 (2016).
[13] N. Rivera and I. Kaminer, Nat. Rev. Phys. **2**, 538 (2020).
[14] H. A. Atwater and A. Polman, Nat. Mater. **9**, 205 (2010).
[15] J. Langer, D. Jimenez de Aberasturi, J. Aizpurua, R. A. Alvarez-Puebla, B. Auguié, J. J. Baumberg, G. C. Bazan, S. E. Bell, A. Boisen, A. G. Brolo *et al.*, ACS Nano **14**, 28 (2020).
[16] J. Homola, Analytic. Bioanalytic. Chem. **377**, 528 (2003).
[17] M. Noginov, G. Zhu, A. Belgrave, R. Bakker, V. Shalaev, E. Narimanov, S. Stout, E. Herz, T. Suteewong, and U. Wiesner, Nature (London) **460**, 1110 (2009).
[18] J. B. Khurgin, Nat. Nanotechnol. **10**, 2 (2015).
[19] M. N. Gjerding, M. Pandey, and K. S. Thygesen, Nat. Commun. **8**, 1 (2017).
[20] G. Cassabois, P. Valvin, and B. Gil, Nat. Photon. **10**, 262 (2016).
[21] See Supplemental Material at http://link.aps.org/supplemental/10.1103/PhysRevMaterials.8.L011001 for additional details regarding higher order loss calculations a derivation of Wannier local field effects and a detailed description of phonon calculations.
[22] L. Weston, D. Wickramaratne, M. Mackoit, A. Alkauskas, and C. G. Van de Walle, Phys. Rev. B **97**, 214104 (2018).
[23] W. Liu, N.-J. Guo, S. Yu, Y. Meng, Z. Li, Y.-Z. Yang, Z.-A. Wang, X.-D. Zeng, L.-K. Xie, J.-F. Wang *et al.*, Mater. Quantum Technol. **2**, 032002 (2022).
[24] G. F. Giuliani and J. J. Quinn, Phys. Rev. Lett. **51**, 919 (1983).
[25] M.-S. Lee and S. D. Mahanti, Phys. Rev. B **85**, 165149 (2012).
[26] G. D. Mahan, *Many-particle Physics* (Springer Science & Business Media, New York, 2013).
[27] A. Agarwal, M. Polini, G. Vignale, and M. E. Flatté, Phys. Rev. B **90**, 155409 (2014).
[28] F. H. da Jornada, L. Xian, A. Rubio, and S. G. Louie, Nat. Commun. **11**, 1013 (2020).
[29] J. P. Perdew, K. Burke, and M. Ernzerhof, Phys. Rev. Lett. **77**, 3865 (1996).
[30] P. A. Dirac, in *Mathematical Proceedings of the Cambridge Philosophical Society* (Cambridge University Press, Cambridge, 1930), Vol. 26, pp. 376–385.
[31] J. P. Perdew, E. R. McMullen, and A. Zunger, Phys. Rev. A **23**, 2785 (1981).
[32] G. Profeta, M. Calandra, and F. Mauri, Nat. Phys. **8**, 131 (2012).
[33] N. Peres, T. Stauber, and A. C. Neto, Europhys. Lett. **84**, 38002 (2008).
[34] S. Gangadharaiah, A. M. Farid, and E. G. Mishchenko, Phys. Rev. Lett. **100**, 166802 (2008).
[35] M. Polini, R. Asgari, G. Borghi, Y. Barlas, T. Pereg-Barnea, and A. H. MacDonald, Phys. Rev. B **77**, 081411(R) (2008).
[36] J. C. G. Henriques, B. Amorim, R. M. Ribeiro, and N. M. R. Peres, Phys. Rev. B **105**, 115421 (2022).
[37] S. Haastrup, M. Strange, M. Pandey, T. Deilmann, P. S. Schmidt, N. F. Hinsche, M. N. Gjerding, D. Torelli, P. M. Larsen, A. C. Riis-Jensen *et al.*, 2D Mater. **5**, 042002 (2018).
[38] J. P. Perdew, A. Ruzsinszky, G. I. Csonka, O. A. Vydrov, G. E. Scuseria, L. A. Constantin, X. Zhou, and K. Burke, Phys. Rev. Lett. **100**, 136406 (2008).
[39] S. L. Adler, Phys. Rev. **126**, 413 (1962).
[40] N. Wiser, Phys. Rev. **129**, 62 (1963).